(see Table II), an accurate determination of k_2 becomes difficult. The values of k_2 presented in Table I were obtained by modeling the profiles of H atom production during the early stage of HNCO decomposition at higher temperatures at which [H] depends most strongly on k_2. The results of a sensitivity analysis carried out for 100 ppm HNCO shocked at T = 2350 K and P = 0.40 atm reveal, for example, the sensitivity coefficient for the H atom defined by $(\partial[H]/\partial k_2)(k_2/[H])$ drops rapidly from 0.96 at t = 1 μs to 0.34 at t = 200 μs (see Figure 3A). On the other hand, for CO, its sensitivity coefficient $(\partial[CO]/\partial k_1)(k_1/[CO])$ remains essentially constant at 1.0–0.92, suggesting that reaction 1 is the predominant source of CO. No other reactions were found to affect CO production rate significantly (see Figure 3B).

Both reactions 1 and 2 are assumed to be effectively in the second-order region. For reaction 1, the result of Hanson et al.,[6] covering a broader range of pressure (0.33–2.2 atm), indicates that the second-order rate constant k_1 is essentially pressure independent.

A brief RRKM calculation carried out by assuming a tight activation complex for reacton 1, which involves a singlet–triplet transition with a barrier of about 85 kcal/mol (comparing with D(HN–CO) = 81 kcal/mol[5]), suggests that the decomposition would be fully second order if the transition coefficient is near unity. If the transmission coefficient is as small as that of the isoelectronic reaction $CO_2 \rightarrow O(^3P) + CO$, $\kappa \sim 10^{-3}$, then reaction 1 would be about 60–70% into the falloff region. Our present results and particularly those of Hanson and co-workers[6] suggest that the transmission coefficient for reaction 1 is probably not much less than unity. A similar calculation for reaction 2, assuming a semirigid transition state with a high-pressure A factor of about 10^{15} s^{-1}, indicates that the decomposition reaction is fully in the second-order region despite the much larger reaction barrier.

Conclusion

We have investigated the kinetics of the thermal decomposition of HNCO in shock waves at temperatures between 2120 and 2570 K by monitoring the production of CO and H atoms. Kinetic modeling of measured product formation profiles provided the second-order rate constants for the two decomposition processes

$$HNCO + Ar \rightarrow NH + CO + Ar \quad (1)$$

$$\rightarrow H + NCO + Ar \quad (2)$$

The modeled values of k_1, which are much greater than those of k_2, agree quantitatively with the ones reported by Hanson, Bowman, and co-workers[6] using entirely different product diagnostics. Combination of both sets of data for k_1 gave rise to the expression

$$k_1 = 10^{15.925\pm0.085} \exp(-42640 \pm 450/T) \quad \text{cm}^3/(\text{mol}\cdot\text{s})$$

covering the temperature range of 1830–3340 K.

Acknowledgment. C. H. Wu is grateful to the Office of Naval Technology for an ONT postdoctoral fellowship. M. C. Lin acknowledges the Office of Naval Research for the support under Contract No. N00014-89-J-1949.

Registry No. HNCO, 420-05-3.

High-Temperature Fast-Flow Reactor Kinetics Studies of the Reactions of AlO with Cl_2 and HCl over Wide Temperature Ranges

Aleksandar G. Slavejkov, Clyde T. Stanton,† and Arthur Fontijn*

High-Temperature Reaction Kinetics Laboratory, Department of Chemical Engineering, Rensselaer Polytechnic Institute, Troy, New York 12180-3590 *(Received: October 6, 1989; In Final Form: January 3, 1990)*

The kinetics of the title reactions have been studied in a high-temperature fast-flow reactor (HTFFR). The relative concentrations of AlO were monitored by laser-induced fluorescence at the $B^2\Sigma$–$X^2\Sigma$ and $C^2\Sigma$–$X^2\Sigma$ transitions. The following $k(T)$ expressions in cm^3 molecule^{-1} s^{-1} are obtained: AlO + Cl_2 (1), $k_1(T) = 3.0 \times 10^{-10} \exp(-1250\ \text{K}/T)$ between 460 and 1160 K; AlO + HCl (2), $k_2(T) = 5.6 \times 10^{-11} \exp(-139\ \text{K}/T)$ between 440 and 1590 K. Confidence limits are given in the text. No fluorescence from a potential four-center product AlCl could be detected. From this it is estimated that less than 5% of the AlO reacted produced AlCl, which indicates that abstraction reactions dominate, i.e., OAlCl + Cl for reaction 1 and OAlCl + H and/or AlOH + Cl for reaction 2.

1. Introduction

Reactions of Al species play a role in several high-temperature environments ranging from rocket exhausts[1] to dust explosions[2] and circumstellar envelopes.[3] To provide a data base for modeling such environments and to guide the development of theory for metallic species reactions, we are engaged in an extensive survey of oxidation reactions of ground-state Al atoms, AlCl ($X^1\Sigma$), and AlO ($X^2\Sigma$).[4-10] Here we report on the first measurements of reactions between AlO ($X^2\Sigma$) and non-oxygen oxidizers. The reactions studied and their thermochemically[11] accessible pathways are

$$AlO + Cl_2 \rightarrow OAlCl + Cl \quad \Delta H^\circ_{298K} = -294 \pm 28\ \text{kJ mol}^{-1} \quad (1a)$$

$$\rightarrow AlCl + OCl \quad \Delta H^\circ_{298K} = -17 \pm 16\ \text{kJ mol}^{-1} \quad (1b)$$

$$AlO + HCl \rightarrow OAlCl + H \quad \Delta H^\circ_{298K} = -105 \pm 28\ \text{kJ mol}^{-1} \quad (2a)$$

$$\rightarrow AlOH + Cl \quad \Delta H^\circ_{298K} = -33 \pm 21\ \text{kJ mol}^{-1} \quad (2b)$$

$$\rightarrow AlCl + OH \quad \Delta H^\circ_{298K} = +13 \pm 16\ \text{kJ mol}^{-1} \quad (2c)$$

2. Technique

The basic HTFFR technique has previously been extensively

† Present address: Naval Research Laboratory, Code 6110, Washington, DC 20375-5000.

(1) Park, C. *Atmos. Environ.* **1976**, *10*, 693.
(2) Ogle, R. A.; Beddow, J. K.; Chen, L. D.; Butler, P. B. *Combust. Sci. Technol.* **1988**, *61*, 75.
(3) Cernichard, J.; Guelin, M. *Astron. Astrophys.* **1987**, *183*, L10.
(4) Rogowski, D. F.; Marshall, P.; Fontijn, A. *J. Phys. Chem.* **1989**, *93*, 1118.
(5) Fontijn, A. *Spectrochim. Acta* **1988**, *43B*, 1075.
(6) Fontijn, A. *Combust. Sci. Technol.* **1986**, *50*, 151.
(7) Rogowski, D. F.; Fontijn, A. *Symp. (Int.) Combust. [Proc.] 21st* **1988**, 943.

0022-3654/90/2094-3347$02.50/0

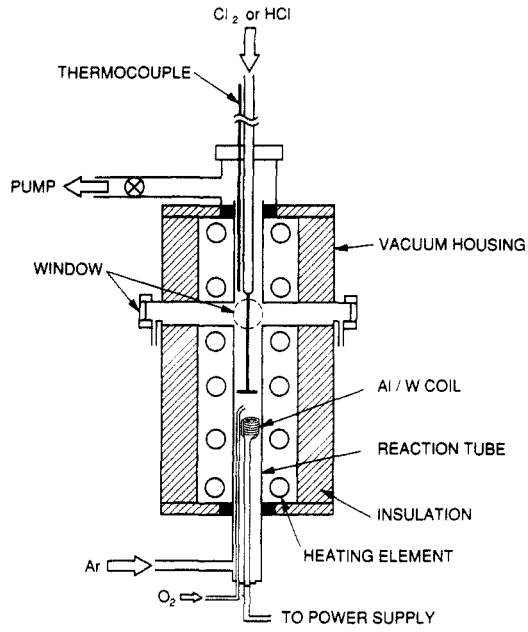

Figure 1. Schematic of the HTFFR used.

described.[12] The reactor used in this work, Figure 1, is slightly modified from that used in our recent studies,[4,8] to allow for AlO production upstream of the observed reaction zone for reactions with non-oxygen oxidants. A vertical 60 cm long, 2.2 cm i.d. reaction tube is heated by SiC resistance heating elements inside an insulated water-cooled vacuum housing. Al is vaporized, in a flow of Ar bath gas, from Al-wetted resistance-heated W coils. About 0.01% (v/v) O_2 is introduced 1 cm downstream of the coil through a Pt tube to produce AlO radicals via[10]

$$Al + O_2 \rightarrow AlO + O \qquad (3)$$

A movable oxidant inlet is used for introduction of Cl_2 or HCl with about 1% of the total Ar carrier gas. Rate coefficient measurements are made in the stationary inlet mode,[7,12] with observed reaction zone lengths of 20 and 10 cm, respectively. The corresponding distances from the O_2 to the Cl_2 or HCl inlet are 8 and 18 cm.

Relative AlO concentrations are monitored by laser-induced fluorescence (LIF) using a pulsed Lambda Physik EMG 101 excimer/FL 2002 dye/KDP doubling crystal combination. Two transitions are used for LIF: $B^2\Sigma$–$X^2\Sigma$ and $C^2\Sigma$–$X^2\Sigma$. In the former case, AlO is pumped on the 464.8-nm (1,0)[13] band and observed at the 486.6-nm (1,1)[13] band through a 482-nm (20 nm fwhm) interference filter. Because of the strong background radiation from the reactor walls, the $B^2\Sigma$–$X^2\Sigma$ system could only be used up to about 1200 K. For kinetic measurements at higher temperatures, as well as a few checks, the $C^2\Sigma$–$X^2\Sigma$ (0,0)[13] transition at 302.2 nm is used to pump and observe AlO through a 301-nm (11 nm fwhm) interference filter. The fluorescence is detected by an EMI 9813 QA photomultiplier tube coupled with a Data Precision Analogic 6000/620 100 MHz transient digitizer.

Preliminary experiments established that Cl_2 and HCl attack alumina at high temperatures; mullite (a SiO_2/Al_2O_3 ceramic), however, appeared resistant under the conditions of this work. To ascertain that no oxidant is lost by wall reaction, two reaction tubes have been used in this work; one constructed from mullite (McDanel MV-30), the other from quartz (GE semiconductor grade).

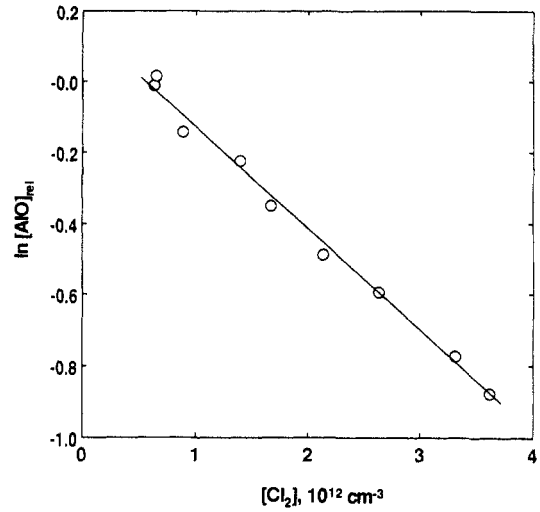

Figure 2. AlO concentration profile vs Cl_2 at a 20-cm Cl_2 inlet to observation port distance. p = 40.7 Torr; v = 37 m s^{-1}; T = 754 K.

The gases used are Ar from the liquid (99.998%), O_2 (1% in Ar, uncertified grade), and Cl_2 (1.01% and 3.00% in Ar, custom grade) all from Linde, and HCl (5.0% in He, certified grade) from Cryogenic.

3. Results

Rate coefficient measurements are made under pseudo-first-order conditions, with AlO as the minor reactant. AlO concentrations, proportional to fluorescence intensities, are measured relative to those obtained at the lowest $[Cl_2]$ or [HCl] used. Plots of such ln $[AlO]_{relative}$ versus $[Cl_2]$ or [HCl] for fixed reaction zone lengths, e.g., Figure 2, yield straight lines with slopes $-kt$, where t is reaction time. For each individual measurement k and σ_k are determined by a weighted linear regression.[7,12,14]

The rate coefficients for the AlO/Cl_2 reaction cover the 460–1160 K range. At the latter temperature equilibrium Cl_2 dissociation would vary from 8% to 20% depending on the $[Cl_2]$ used. Because of its short residence time Cl_2 dissociation does not reach equilibrium, and no drop off in k values is observed. However, above about 1160 K a sharp drop off in the rate coefficients was detected, which can be attributed to significant Cl_2 dissociation. Measurements on the AlO/HCl reaction are made from 440 to 1590 K. At the highest temperature HCl equilibrium dissociation would be 20%. However, for reasons similar to those for the AlO/Cl_2 reaction, no drop off in rate coefficients was observed, indicating that dissociation of HCl is slow at those temperatures.

The individual k_1 and k_2 measurements and the conditions under which they were obtained are summarized in Tables I and II, respectively. It may be seen that the rate coefficient values are independent of the average total concentration $[\bar{M}]$, average gas velocity $\bar{v}$, the observed reaction zone length, the initial fluorescence intensity F (a measure of the initial [AlO]), and whether a quartz or mullite reaction tube was used. While the average of the measurements made on reaction 2 using the $C^2\Sigma$–$X^2\Sigma$ transition show slightly higher values than those made on the $B^2\Sigma$–$X^2\Sigma$ transition, individual measurements overlap.

Within the scatter of data no curvature is evident in the Arrhenius plots, Figures 3 and 4. The observed temperature dependences of the rate coefficients for each reaction are best described in Arrhenius form

$$k(T) = A \exp(-B/T) \qquad (4)$$

(8) Rogowski, D. F.; English, A. J.; Fontijn, A. *J. Phys. Chem.* **1986**, *90*, 1688.
(9) Rogowski, D. F.; Fontijn, A. *Chem. Phys. Lett.* **1986**, *132*, 413.
(10) Fontijn, A.; Felder, W.; Houghton, J. J. *Symp. (Int.) Combust., [Proc.] 16th* **1977**, 871.
(11) The thermochemical data are obtained from: Chase, M. W., Jr.; Davies, C. A.; Downey, Jr.; Frurip, D. J.; McDonald, R. A.; Syverup, A. N. *JANAF Thermochemical Tables, J. Phys. Chem. Ref. Data* **1985**, *14*, supplement No. 1.
(12) Fontijn, A.; Felder, W. In *Reactive Intermediates in the Gas Phase. Generation and Monitoring*; Setser, D. W., Ed.; Academic Press: New York, 1979; Chapter 2.
(13) Pearse, R. W. B.; Gaydon, A. G. *The Identification of Molecular Spectra*; Chapman and Hall: London, 1976; p 41.
(14) Bevington, P. R. *Data Reduction and Error Analysis for the Physical Sciences*; McGraw-Hill: New York, 1969; Chapter 1.

TABLE I: Summary of Rate Coefficient Measurements of AlO + Cl_2[a]

reaction zone length, cm	$\bar{P}$,[b] Torr	$[\bar{M}]$, 10^{17} cm^{-3}	$[Cl_2]$ range, 10^{12} cm^{-3}		F[c]	$\bar{v}$, m/s	T, K	k, 10^{-11} cm^3 molecule^{-1} s^{-1}	$\pm\sigma_k$, 10^{-11} cm^3 molecule^{-1} s^{-1}
20	20.5	2.6	0.62	3.6	65	40	763	5.53[d]	0.62
20	20.5	2.6	0.57	3.0	70	40	763	5.43[d]	0.44
10	20.5	2.6	1.1	8.1	84	40	753	4.44[d]	0.30
10	20.6	2.6	1.0	9.0	87	40	753	4.23[d]	0.45
10	40.7	5.2	1.2	5.0	82	37	751	7.41[d]	0.64
10	40.7	5.3	1.1	6.1	88	37	747	5.48[d]	0.32
20	40.7	5.2	0.64	3.7	72	37	754	5.09[d]	0.30
20	40.7	5.2	0.62	4.3	74	37	753	5.35[d]	0.27
20	10.6	2.2	1.6	8.6	63	48	470	2.36[d]	0.32
20	10.6	2.2	1.7	9.4	76	48	471	2.33[d]	0.21
10	10.6	2.2	1.9	14	78	47	460	1.64[d]	0.17
10	10.6	2.2	1.7	14	75	47	462	2.04[d]	0.24
20	20.3	4.1	0.91	7.1	46	47	473	2.66[d]	0.21
20	11.9	1.7	1.5	9.3	180	59	656	4.16[d]	0.39
20	11.9	1.7	1.2	10	190	60	662	4.12[d]	0.38
10	11.9	1.7	1.4	11	190	59	660	5.74[d]	0.50
10	11.9	1.7	1.3	11	190	59	664	5.50[d]	0.50
10	21.4	3.1	1.3	10	120	62	670	4.61[d]	0.31
10	21.4	3.1	1.4	10	120	63	673	4.18[d]	0.27
20	21.4	3.0	1.2	10	100	64	685	4.13[d]	0.30
20	21.4	3.0	1.5	10	100	64	690	4.20[d]	0.23
20	20.0	3.3	0.93	7.9	100	37	591	2.86[d]	0.24
20	20.4	3.3	0.93	8.8	110	36	597	1.92[d]	0.14
10	20.4	3.3	2.5	14	110	36	590	4.32[d]	0.34
10	20.4	3.3	2.0	13	130	37	600	3.94[d]	0.37
10	11.0	1.8	1.3	10	240	69	601	4.96[d]	0.44
10	11.0	1.8	1.2	10	210	69	602	5.35[d]	0.58
20	11.0	1.7	1.3	9.4	180	71	617	3.72[d]	0.32
20	11.0	1.7	1.2	8.9	190	71	626	4.27[d]	0.40
20	16.5	1.5	0.73	3.3	50	84	1083	10.90[d]	0.70
20	16.5	1.5	0.75	3.7	44	85	1086	11.40[d]	0.84
10	16.5	1.5	0.72	7.0	56	85	1084	9.09[d]	0.69
10	16.5	1.5	0.72	7.8	55	85	1087	9.92[d]	0.80
10	31.6	2.8	1.0	7.2	79	66	1082	14.90[d]	1.21
10	31.6	2.8	1.1	7.3	77	66	1076	14.90[d]	1.08
20	11.5	1.9	1.4	7.4	87	64	582	3.60[d]	0.33
20	11.5	1.9	1.2	8.1	82	65	589	4.08[d]	0.35
10	11.4	2.0	1.5	11	66	61	546	4.15[d]	0.46
10	11.4	2.1	1.4	11	68	59	531	3.89[d]	0.39
10	21.1	3.9	2.0	8.9	78	47	528	5.36[d]	0.41
10	21.1	3.9	1.8	9.6	80	47	527	4.42[d]	0.56
20	21.1	3.8	1.7	7.6	95	47	532	3.70[d]	0.24
20	21.1	3.8	1.9	8.8	93	47	530	3.84[d]	0.27
20	21.1	2.4	1.0	4.3	95	49	840	7.22[d]	0.45
20	21.1	2.4	0.91	4.0	93	49	848	6.66[d]	0.52
10	21.0	2.4	1.6	7.7	90	49	843	7.03[d]	0.49
10	21.1	2.4	1.6	7.3	75	50	854	9.23[d]	0.66
20	21.1	2.4	1.1	5.4	100	71	864	6.72[d]	0.36
20	21.1	2.4	1.3	5.4	100	71	865	6.38[d]	0.41
20	15.9	1.6	1.2	7.7	250	83	955	8.11[d]	0.56
20	16.0	1.6	1.1	7.8	260	83	961	6.60[d]	0.46
10	16.0	1.6	1.0	7.7	250	83	958	6.05[d]	0.51
10	16.0	1.6	1.1	7.8	230	83	962	6.06[d]	0.52
20	15.8	2.9	2.1	9.2	89	40	528	2.03[d]	0.15
20	15.8	2.9	2.1	9.4	85	40	527	1.82[d]	0.23
10	15.9	3.0	2.3	16	120	38	514	2.13[d]	0.22
10	15.9	3.0	2.4	17	120	38	510	2.17[d]	0.24
20	21.3	1.8	1.0	6.1	110	87	1135	13.00[e]	1.13
10	21.3	1.8	1.0	7.4	110	87	1140	9.15[e]	0.89
10	20.4	2.0	1.4	9.8	110	65	975	5.34[e]	0.50
20	20.3	2.0	0.65	5.0	100	65	974	8.10[e]	0.51
20	16.5	1.8	0.66	4.4	120	73	885	7.08[e]	0.49
20	11.1	1.6	0.57	5.1	94	54	671	6.48[e]	0.62
20	11.0	1.4	0.66	6.1	210	60	736	5.93[e]	0.54
20	12.0	1.6	1.2	6.5	210	67	714	2.43[e]	0.30
20	16.6	2.7	1.0	7.9	85	40	584	3.23[e]	0.23
20	19.4	1.8	0.87	5.6	49	54	1047	8.48[f]	0.87
20	19.4	1.8	1.2	6.8	64	54	1050	8.82[f]	0.56
10	19.4	1.8	1.5	13	37	54	1058	8.77[f]	0.66
10	19.4	1.8	1.5	12	26	55	1060	8.86[f]	0.68
20	10.9	1.1	0.52	5.2	32	65	1003	8.95[f]	0.86
20	10.6	1.2	0.69	5.6	64	60	891	6.83[f]	0.69
20	10.6	1.1	0.64	5.6	64	60	900	6.99[f]	0.72
20	10.5	1.2	0.90	6.3	43	55	824	5.89[f]	0.65
20	10.5	1.2	0.63	5.5	39	56	830	7.05[f]	0.77
10	11.8	1.0	0.81	6.5	69	100	1164	12.10[f]	1.35

[a] The measurements are reported in the sequence in which they were obtained. [b] 1 Torr = 133.3 Pa. [c] In arbitrary units. [d] Data obtained by using the $B^2\Sigma$–$X^2\Sigma$ transition and the mullite reaction tube. [e] Data obtained by using the $B^2\Sigma$–$X^2\Sigma$ transition and the quartz reaction tube. [f] Data obtained by using the $C^2\Sigma$–$X^2\Sigma$ transition and the mullite reaction tube.

TABLE II: Summary of Rate Coefficient Measurements of AlO + HCl[a]

reaction zone length, cm	$\bar{P}$,[b] Torr	[M], 10^{17} cm^{-3}	[HCl] range, 10^{12} cm^{-3}		F[c]	$\bar{v}$, m/s	T, K	k, 10^{-11} cm^3 molecule^{-1} s^{-1}	$\pm\sigma_k$, 10^{-11} cm^3 molecule^{-1} s^{-1}
20	14.6	1.5	2.9	20	110	75	961	4.44[d]	0.31
10	14.6	1.5	3.0	22	81	76	967	5.70[d]	0.60
20	14.6	1.5	2.8	19	120	76	968	5.95[d]	0.40
10	14.5	1.4	2.6	20	100	76	976	6.38[d]	0.49
20	20.1	2.6	2.8	23	190	43	747	2.56[d]	0.16
10	20.1	2.6	2.6	24	160	43	738	3.71[d]	0.27
20	4.6	0.60	1.4	11	140	90	733	6.48[d]	1.16
10	4.6	0.61	2.2	13	140	88	721	6.64[d]	1.19
20	4.7	0.61	1.4	13	140	88	735	6.01[d]	1.04
10	14.2	1.5	1.6	9.3	77	72	915	4.54[d]	0.49
20	14.2	1.5	1.9	9.4	75	72	919	6.36[d]	0.57
20	20.4	2.2	1.8	11	310	62	900	2.78[d]	0.19
10	20.3	2.2	1.8	11	210	62	902	4.24[d]	0.37
20	20.3	2.2	2.2	10	150	63	909	2.65[d]	0.15
10	20.3	2.2	1.8	11	160	63	910	4.20[d]	0.39
20	10.3	0.91	1.2	9.9	90	71	1102	8.96[d]	0.90
10	30.4	2.6	2.6	13	95	50	1127	6.18[d]	0.62
20	30.3	2.6	2.2	14	99	49	1118	3.52[d]	0.40
10	19.9	1.8	1.3	9.4	64	71	1079	4.43[d]	0.57
20	19.9	1.8	1.7	9.8	49	71	1072	2.86[d]	0.24
10	19.9	1.8	1.5	9.8	59	71	1077	2.89[d]	0.24
20	10.8	1.2	1.9	9.3	110	70	884	6.83[d]	0.63
10	10.8	1.2	1.9	9.9	100	70	887	5.85[d]	0.67
20	10.7	1.2	1.5	9.8	94	71	887	3.34[d]	0.33
20	8.2	1.8	2.5	15	62	45	440	5.07[d]	0.56
10	4.5	0.77	2.0	10	130	67	570	7.65[d]	1.43
20	4.6	0.75	1.7	9.8	62	69	592	4.72[d]	0.95
10	4.5	0.74	1.6	9.2	32	69	590	2.80[d]	0.62
20	4.6	0.72	1.1	6.9	19	71	613	2.63[d]	0.59
20	10.7	0.86	0.80	9.0	110	102	1196	6.27[d]	0.60
10	10.8	0.87	0.87	4.9	37	139	1201	5.32[d]	1.68
20	10.8	0.88	1.0	6.8	70	138	1190	4.18[d]	0.46
10	10.8	0.86	0.75	6.7	56	140	1204	5.71[d]	0.87
20	5.0	0.40	1.2	6.1	33	106	1209	7.91[d]	1.55
10	5.1	0.40	1.2	8.3	60	115	1220	4.38[d]	0.90
20	5.1	0.40	0.96	7.8	60	117	1226	3.19[d]	0.64
10	5.1	0.40	1.1	10	76	120	1220	3.62[d]	0.68
20	14.7	1.4	1.3	8.9	160	80	1053	5.48[e]	0.60
10	15.8	1.5	1.8	9.3	100	75	1056	7.43[e]	0.68
10	14.8	1.4	1.6	8.8	40	80	1058	4.58[e]	0.59
20	10.8	1.0	1.3	8.5	57	82	1057	4.50[e]	0.77
20	10.7	0.97	1.6	8.4	42	84	1072	2.73[e]	0.34
10	10.7	0.96	1.7	8.2	52	84	1073	2.76[e]	0.32
20	19.4	1.9	2.0	11	140	59	969	4.84[e]	0.35
10	19.4	1.9	2.1	12	93	59	967	4.71[e]	0.36
20	10.5	1.3	1.7	11	56	63	772	7.95[e]	0.79
20	10.5	1.3	1.6	10	51	64	782	5.62[e]	0.58
10	6.8	1.4	2.8	17	29	39	487	3.67[e]	0.51
20	6.8	1.2	1.8	14	17	43	536	3.89[e]	0.56
10	6.8	1.3	1.7	12	16	41	506	3.70[e]	0.52
20	6.8	1.1	2.1	14	58	47	579	3.86[e]	0.53
20	24.8	3.7	2.0	9.5	98	36	649	5.95[e]	0.81
10	24.8	3.8	2.0	9.6	110	35	635	6.92[e]	0.47
20	24.8	3.6	1.9	9.4	100	37	656	4.96[e]	0.32
10	24.8	3.7	2.3	9.7	120	36	640	5.90[e]	0.55
10	5.4	1.2	1.4	2.5	30	43	457	4.73[e]	0.88
20	10.7	1.8	1.7	7.3	39	48	566	2.40[e]	0.35
10	10.7	1.9	1.8	7.6	43	46	540	4.86[e]	0.60
20	19.5	1.5	0.89	7.5	25	69	1221	5.21[f]	0.44
20	15.7	1.4	0.93	6.0	40	75	1052	4.77[f]	0.42
10	15.7	1.4	0.74	6.2	27	75	1052	7.29[f]	1.42
20	11.6	0.74	0.52	5.5	78	101	1514	6.39[f]	0.60
20	11.6	0.74	0.48	6.0	110	101	1514	6.95[f]	0.69
20	15.1	0.96	0.74	6.0	73	75	1529	6.77[f]	0.69
10	15.2	0.95	0.67	6.1	68	76	1543	6.55[f]	0.73
20	15.2	0.96	0.78	6.3	88	75	1529	4.63[f]	0.38
10	15.2	0.95	0.64	6.1	73	76	1543	8.03[f]	1.06
20	15.7	1.7	1.0	8.9	18	62	872	5.79[f]	0.60
10	15.7	1.7	1.1	5.1	22	62	880	5.23[f]	1.26
20	30.7	3.3	1.1	3.5	7	60	894	7.06[f]	0.72
20	30.7	3.3	1.0	4.7	6	60	894	7.08[f]	0.82
20	20.6	1.4	0.96	6.7	44	85	1468	6.31[f]	0.59
10	20.6	1.3	0.922	9.1	46	86	1480	4.66[f]	0.41
20	20.4	1.3	0.96	6.2	45	87	1498	4.51[f]	0.34
10	20.3	1.3	0.96	8.7	40	89	1510	6.84[f]	0.55

[a] The measurements are reported in the sequence in which they were obtained. [b] 1 Torr = 133.3 Pa. [c] In arbitrary units. [d] Data obtained by using the $B^2\Sigma$–$X^2\Sigma$ transition and the mullite reaction tube. [e] Data obtained by using the $B^2\Sigma$–$X^2\Sigma$ transition and the quartz reaction tube. [f] Data obtained by using the $C^2\Sigma$–$X^2\Sigma$ transition and the mullite reaction tube.

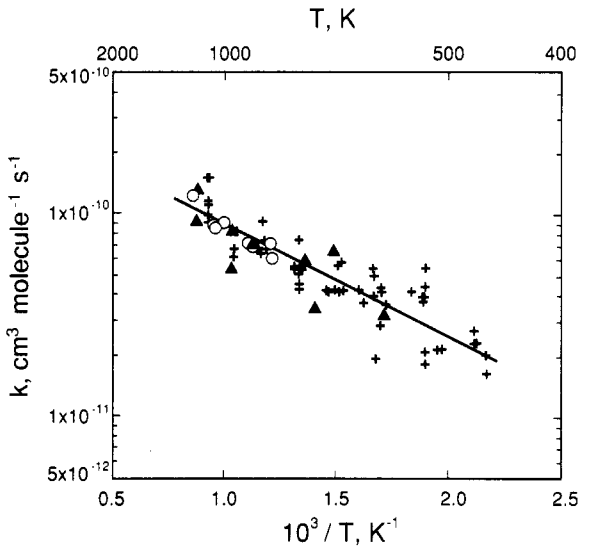

Figure 3. Rate coefficient data for the AlO/Cl_2 reaction: +, $B^2\Sigma$-$X^2\Sigma$ LIF, mullite reaction tube; Δ, $B^2\Sigma$-$X^2\Sigma$ LIF, quartz reaction tube; O, $C^2\Sigma$-$X^2\Sigma$ LIF, mullite reaction tube.

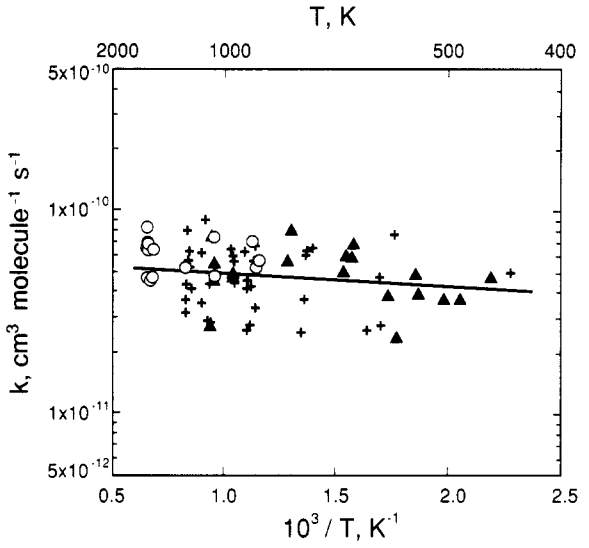

Figure 4. Rate coefficient data for the AlO/HCl reaction: +, $B^2\Sigma$-$X^2\Sigma$ LIF, mullite reaction tube; Δ, $B^2\Sigma$-$X^2\Sigma$ LIF, quartz reaction tube; O, $C^2\Sigma$-$X^2\Sigma$ LIF, mullite reaction tube.

The parameters A and B are obtained by using the usual regression analysis.[7,12,14] For reaction 1 the best fit expression is

$$k_1(T) = 3.0 \times 10^{-10} \exp(-1250\ \mathrm{K}/T)\ \mathrm{cm^3\ molecule^{-1}\ s^{-1}} \quad (5)$$

with the variances and covariance;[15] ${\sigma_{A_1}}^2/{A_1}^2 = 0.011$, ${\sigma_{B_1}}^2 = 6100$, $\sigma_{AB_1}/A_1 = 7.8$. The resulting $2\sigma_{k_1}(T)$ confidence levels which include a 10% systematic error in the flow profile factor[12,16] vary from ±25% at 460 K to ±21% in the range 700–1160 K. The expression for reaction 2 is

$$k_2(T) = 5.6 \times 10^{-11} \exp(-139\ \mathrm{K}/T)\ \mathrm{cm^3\ molecule^{-1}\ s^{-1}} \quad (6)$$

The variances and covariance are ${\sigma_{A_2}}^2/{A_2}^2 = 0.018$, ${\sigma_{B_2}}^2 = 14500$, $\sigma_{AB_2}/A_2 = 15.5$. The resulting $2\sigma_{k_2}(T)$ confidence levels vary from ±36% at 440 K to ±23% in the range 700–1590 K.

To obtain information on the reaction products, we looked for AlCl LIF at the 261.4-nm A–X(0,0) transition. None could be found in either the Cl_2 or HCl reaction at a number of reaction zone lengths (5–25 cm) and temperatures in the 900–1100 K range. To ascertain that if AlCl had been present it could have been detected, the O_2 flow was stopped and Cl_2 or HCl was added. Strong AlCl fluorescence from the Al + Cl_2, HCl reactions[4] was then observed. On this basis we estimate any AlCl product paths to represent less than 5% of reactions 1 and 2.

4. Discussion

The apparent absence of AlCl identifies the OAlCl formation reaction 1a as the major path for the Cl_2 reaction and (2a) as a likely path for the HCl reaction (in any case (2b) is an abstraction reaction too). Thus abstraction reactions dominate and the four-center paths (1b) and (2c) contribute negligibly, as usual experience with reactions of nonmetallics would have led one to expect. However, Silver et al.[17] have given evidence that the reaction NaO + HCl proceeds to NaCl + OH at near gas kinetic rates at room temperature. Thus, for metallic elements four-center reactions must be considered. The amphoteric element Al in this respect thus resembles a metalloid more than an alkali metal.

It is interesting to compare the low activation energies for formation of OAlCl from $AlO(X^2\Sigma)$ in the present work, to the high activation energies of $AlCl(X^1\Sigma) + O_2$ (E_a/R = 3400 K) where OAlCl + O is the most probable product channel,[18] and $AlCl(X^1\Sigma) + CO_2$ (E_a/R = 7550 K)[9] where OAlCl + CO is the only thermochemically accessible channel. Apparently, the AlO doublet radical can participate directly in a free-radical reaction, whereas energy is required to decouple an electron pair in AlCl reactions. On this basis the activation energy for reaction 1 is normal; however, that for reaction 2 is strikingly low. Near zero negative temperature dependences have been observed in two previously studied AlO reactions, i.e., those with CO_2 and O_2. For those reactions $k(T)$ of $2.5 \times 10^{-14} \exp(400\ \mathrm{K}/T)$ and $2.3 \times 10^{-13} \exp(333\ \mathrm{K}/T)$, respectively, were found.[8,10] Those results can be explained in terms of the most frequent cause for such observations, i.e., formation of an intermediate complex, which dissociates preferentially to reactants rather than to products.[19] The small preexponentials are a good indication for such a mechanism. However, reaction 2 has a large A factor; hence another mechanism must operate there. A possible explanation lies in the fact that both AlO and HCl are strong dipoles. The complex resulting from dipole–dipole interactions would live for several rotations and the increased reaction probability during that period would result in large A factors. With increasing temperature the increased centrifugal barrier[20,21] and the rotational energy of the reactants would reduce the fraction of successful collisions, while the collision frequency increases. The result of these opposing effects is a small temperature dependence.

To attempt to establish how well current theory can assist in estimating $k_1(T)$ and $k_2(T)$, we can start with the standard collision theory expression for thermal energy distributions[21]

$$k(T) = \pi d^2 (8RT/\pi\mu)^{1/2} \exp(-E_0/RT) \quad (7)$$

where E_0 is the threshold energy. Following Plane and Saltzman's approximation[22] we substitute the maximum impact parameter b_{max} for d, where[21]

$${b_{max}}^2 = (3/2)^{2/3}(3C_6/E_T)^{1/3} \quad (8)$$

The parameter C_6 can then be estimated from all the long-range interactions involved, i.e., for reaction 1, dispersive and dipole-induced dipole, and for reaction 2, these plus dipole–dipole interactions. Using the usual formulas for these forces[22] and lit-

(15) Wentworth, W. E. *J. Chem. Educ.* **1965**, *42*, 96.
(16) Fontijn, A.; Felder, W. *J. Phys. Chem.* **1979**, *83*, 24.
(17) Silver, J. A.; Stanton, A. C.; Zahniser, M. S.; Kolb, C. E. *J. Phys. Chem.* **1984**, *88*, 3123.
(18) Slavejkov, A. G.; Fontijn, A. Manuscript in preparation.
(19) Fontijn, A.; Zellner, R. In *Reactions of Small Transient Species. Kinetics and Energetics*: Fontijn, A., Clyne, M. A. A., Eds.; Academic: London, 1983; Chapter 1.
(20) Levine, R. D.; Bernstein, R. B. *Molecular Reaction Dynamics and Chemical Reactivity*; Oxford University Press: Oxford, U.K., 1987; pp 43, 420.
(21) Smith, I. W. M. *Kinetics and Dynamics of Elementary Gas Reactions*; Butterworth: London, 1980; Chapter 3.
(22) Plane, J. M. C.; Saltzman, E. S. *J. Phys. Chem.* **1987**, *87*, 4606.

erature values for the terms involved[23] leads to

$$k_1(T) = 3.3 \times 10^{-10} T^{1/6} \exp(-E_0/RT) \text{ cm}^3 \text{ molecule}^{-1} \text{ s}^{-1} \quad (9)$$

This preexponential is within about a factor of 3 of that found experimentally, eq 5, which appears reasonable. However, for reaction 2 we obtain

$$k_2(T) = [4.3T^{-1/2} + 0.035T^{1/2}]^{1/3} \times 10^{-9} \exp(-E_0/RT) \text{ cm}^3 \text{ molecule}^{-1} \text{ s}^{-1} \quad (10)$$

where the preexponential is about a factor 18 higher than given by eq 6. To allow a more complete comparison to experiment, we follow a semiempirical approach to finding E_0 by setting expressions 9 and 10 equal to (5) and (6), respectively, at the midpoint temperatures of the experiments. This gives E_0/R = 2252 and 3175 K, for reactions 1 and 2, respectively, much larger than observed. This poor agreement also prevents a more rigorous test of the above explanation for the very small T dependence of reaction 2. We have considered using transition-state theory but lack a foundation for estimating geometry and vibrational frequencies of the transition-state complex.

As both reactions 1 and 2 are fast, they should be suitable candidates for molecular beam studies, which may be expected to be able to yield a more quantitative understanding than can be provided here.

Acknowledgment. This work was supported under grant AFOSR 89-0086. Clyde Stanton's participation was funded by NRL through ONR grant N00014-88-J-1109. We thank Drs. C. E. Kolb, M. E. Jacox and P. Davidovits for helpful discussions. Chris Childs assisted with some of the experiments.

Registry No. AlO, 14457-64-8; Cl_2, 7782-50-5; HCl, 7647-01-0.

(23) The values used for the calculation are[24-26] $\alpha_{AlO} = 26.5 \times 10^{-30}$ m^3, $\alpha_{Cl_2} = 4.6 \times 10^{-30}$ m^3, $\alpha_{HCl} = 2.6 \times 10^{-30}$ m^3, $p_{AlO} = 14.2 \times 10^{-30}$ C m, and $p_{HCl} = 3.6 \times 10^{-30}$ C m, where α is the polarizability and p the dipole moment.

(24) Pandey, A. N.; Mithal, A. K.; Shukla, M. M.; Singh, G. C. *Indian J. Pure Appl. Phys.* **1973**, *11*, 69.
(25) Das, G.; Janis, T.; Wahl, A. C. *J. Phys. Chem.* **1974**, *61*, 1273.
(26) Weast, R. C., Astle, M. J., Beyer, W. H., Eds. *CRC Handbook of Chemistry and Physics*, 66th ed.; CRC Press: Boca Raton, FL 1985; pp E-61, E-69.

Pressure Dependence of the C_2H_4 Yield from the Reaction $C_2H_5 + O_2$

E. W. Kaiser,* I. M. Lorkovic,† and T. J. Wallington

Chemistry Department, Ford Motor Company, Scientific Research Laboratories E-3083, Dearborn, Michigan 48121-2053 *(Received: September 29, 1989; In Final Form: December 16, 1989)*

The yield of C_2H_4 formed during the reaction of C_2H_5 with O_2 has been determined at 298 K for pressures from 1.0 to 6000 Torr. Ethyl radicals were formed by UV irradiation of mixtures of Cl_2, C_2H_6, O_2, and N_2 in either a Pyrex (1.0–1500 Torr) or a stainless steel (760–6000 Torr) reactor. The ethylene yield decreased with increasing pressure from 12% of the C_2H_5 consumed by O_2 at 1 Torr to 0.02% at 6000 Torr, following a $P^{-0.8\pm0.1}$ pressure dependence in air. These data support the formation of C_2H_4 via an excited ethylperoxy intermediate at 298 K and place an upper limit of 1.4×10^{-15} cm^3/(molecule·s) on the rate constant for formation of C_2H_4 via a direct abstraction reaction. Experiments performed in He diluent showed the same $P^{-0.8}$ dependence over the range 3–1500 Torr, but the absolute C_2H_4 yields were a factor of 1.7 larger at all pressures. This indicates that He has a third-body efficiency approximately a factor of 0.45 smaller than that of air for deactivation of excited $C_2H_5O_2$ radicals.

Introduction

The mechanism by which C_2H_5 reacts with O_2 to form C_2H_4 is of interest theoretically and experimentally[1-6] because of its influence on combustion and atmospheric chemistry. Two channels could yield C_2H_4 from this reaction: (1) direct abstraction

$$C_2H_5 + O_2 \rightarrow C_2H_4 + HO_2 \quad (1)$$

or (2) a coupled-path mechanism via an excited $C_2H_5O_2$ intermediate as proposed by several authors (see the thorough review in ref 5) and supported by the experiments of Slagle et al.[1] This latter reaction mechanism can be written in simplified form using the Lindemann scheme:

$$C_2H_5 + O_2 = C_2H_5O_2^* \quad (2a)$$

$$C_2H_5O_2^* \rightarrow C_2H_4 + HO_2 \quad (2b)$$

$$C_2H_5O_2^* + M \rightarrow C_2H_5O_2 + M \quad (2c)$$

The nature of the activated complex, $C_2H_5O_2^*$, is the subject of ongoing investigation. Several authors (e.g., refs 1 and 5) propose that the reaction proceeds via a $C_2H_4O_2H$ radical intermediate, while McAdam and Walker[6] suggest that a direct decomposition of the cyclic transition state is the preferred path. Because our measurements cannot distinguish between these two reaction channels, we have chosen to write the mechanism in its simplest form. However, we emphasize that the $C_2H_5O_2$ and $C_2H_5O_2^*$ species in reaction 2 may consist of peroxy- and/or hydroperoxy-ethyl radical intermediates.

Studies 2–5 at room temperature have shown a decreasing C_2H_4 yield with increasing pressure in agreement with mechanism 2. However, each of these sets of data spans a limited pressure range of a factor of 2–10, and only upper limits to the C_2H_4 yield have been obtained for pressures greater than 100 Torr. Thus, the precise nature of the pressure dependence is not well established, and the presence of a pressure-independent yield at sufficiently high pressures, which would indicate the existence of channel 1, cannot be ruled out.

Experimental Section

The experiments were performed in two reactors: a 500-cm^3 Pyrex flask for pressures from 1.0 to 1500 Torr and a 50-cm^3 stainless steel reactor with quartz windows for pressures from 760 to 6000 Torr. Ethyl radicals were generated in both reactors according to the reaction

† Current address: Department of Chemistry, Massachusetts Institute of Technology, Cambridge, MA.

(1) Slagle, I. R.; Feng, Q.; Gutman, D. *J. Phys. Chem.* **1984**, *88*, 3648–3653.
(2) Kaiser, E. W.; Rimai, L.; Wallington, T. J. *J. Phys. Chem.* **1989**, *93*, 4094–4098.
(3) Wallington, T. J.; Andino, J. M.; Kaiser, E. W.; Japar, S. M. *Int. J. Chem. Kinet.* **1989**, *21*, 1113–1122.
(4) Plumb, I. C.; Ryan, K. R. *Int. J. Chem. Kinet.* **1981**, *13*, 1011–1028.
(5) Wagner, A. F.; Slagle, I. R.; Sarzynski, D.; Gutman, D. *J. Phys. Chem.*, in press.
(6) McAdam, K. G.; Walker, R. W. *J. Chem. Soc., Faraday Trans. 2* **1987**, 1509.

0022-3654/90/2094-3352$02.50/0